Available online at www.sciencedirect.com
SCIENCE DIRECT
Polymer 47 (2006) 5602–5609
polymer
www.elsevier.com/locate/polymer

# Novel aspects of microindentation hardness in very low crystallinity ethylene-1-octene copolymers: A model for deformation

A. Flores [a], V.B.F. Mathot [b], G.H. Michler [c], R. Adhikari [c], F.J. Baltá Calleja [a,*]

[a] *Instituto de Estructura de la Materia, CSIC, Serrano 119, 28006 Madrid, Spain*
[b] *DSM Research, PO Box 18, 6160 MD, Geleen, The Netherlands*
[c] *Department of Engineering, Institute of Materials Science, Martin-Luther Universität Halle-Wittenberg, D-06099 Halle/Saale, Germany*

Received 2 November 2004; accepted 16 December 2004
Available online 16 May 2006

Dedicated to Prof. D.C. Bassett on occasion of his retirement

**Abstract**

The microindentation hardness, $H$ (critical stress required to mechanically deform a material), of a series of homogeneous ethylene-1-octene copolymers with high comonomer content and low crystallinities ($\alpha < 0.4$) has been determined. The $H$ values obtained for the series of ethylene–octene copolymers are found to be notably smaller than those of linear and commercial short-chain branched polyethylene. The microhardness of an ethylene based material having a nearly zero crystallinity value has been measured for the first time. Results are discussed using a description of hardness in the light of the crystal characteristics (surface free energy and dimensions) and the energy required for plastic deformation. In high crystallinity materials, lamellar shearing and crystal fracture mechanisms prevail. In contrast, resistance to deformation for low crystallinity ethylene-1-octene copolymers ($\alpha = 0.074$–$0.22$), showing well-developed indentations, involves the following deformation modes: (i) bond rotation of the molecules within the amorphous phase, (ii) elastic compression and bending of the nanocrystals and (iii) slippage of the dispersed nanocrystals through the amorphous matrix. The extent of the latter deformation mechanism should be modulated by the viscosity of the amorphous phase. According to these deformation mechanisms, the average dimensions of the nanocrystals after deformation remain practically unaffected. Within this context, it is shown that the dissipated energy during deformation, as derived from the mechanical parameter, $b$, decreases with increasing short-chain branching content.


*Keywords:* Ethylene-1-octene copolymers; Microhardness; Deformation mechanisms

## 1. Introduction

Microindentation hardness is one of the simplest ways to probe the mechanical properties of a polymer surface [1,2]. The method is based on the local deformation produced at a microscopic scale by a sharp indenter. In homogenous systems, microhardness is a measure of the mechanical properties of the bulk material, and can be easily related to the yield stress and the elastic modulus [3,4]. During an indentation cycle, elastic and plastic deformations are usually generated during the application of the load. Upon unloading, an instant elastic recovery takes place. Microhardness, as determined from optical measurement of the residual impression left behind upon load withdrawal, is related to the permanent plastic strains induced in the material.

The deformation mechanisms in polymer materials during and upon indentation have been discussed in the past [5]. However, there are still some questions, which need further clarification. Recent combined microindentation and micro-diffraction experiments carried out on single ultra-high molecular weight polyethylene, nylon 66 and isotactic polypropylene fibers using a synchrotron source suggest that the main structural change occurring during indentation is associated with local changes in the crystal orientation, which partially recover upon load release [6,7]. It has also been shown that plastic deformation may also involve a partial polymorphic transformation [6,7].

In oriented and isotropic semicrystalline polymer systems, it is known that both the crystalline and amorphous regions contribute to the material resistance to plastic deformation. Until now substantial experimental evidence has been accumulated for the microhardness, $H$, of a semicrystalline

* Corresponding author.
*E-mail address:* embalta@iem.cfmac.csic.es (F.J. Baltá Calleja).

0032-3861/$ - see front matter © 2006 Elsevier Ltd. All rights reserved.
doi:10.1016/j.polymer.2004.12.065

polymer accounting for the individual contributions of the crystalline and non-crystalline components following the additive rule (parallel model) [1,2]:

$$H = H_c\alpha + H_a(1-\alpha) \quad (1)$$

$H_c$ and $H_a$ being the hardness of the crystalline and amorphous regions, respectively, and $\alpha$ the volume fraction of crystalline material. $H_c$ depends—amongst other parameters—on the nanocrystal morphology. On the other hand, previous room temperature (RT) microhardness studies of polymers exhibiting a glass transition temperature, $T_g$, well below RT, have assumed that $H_a \approx 0$ [1,2]. The microhardness behavior of glassy poly(ethylene terephthalate) (PET) as a function of temperature reveals, indeed, a conspicuous $H$-decrease as the $T_g$ value is approached, leading to extremely small hardness values ($H \approx 5$ MPa) a few degrees above $T_g$ ($\approx 100$ °C), before crystallization takes place [8]. In case of polyethylene (PE), it has been widely assumed that $H_a \approx 0$ at RT, although there has been no direct evidence so far [1,2].

The thermal behavior, morphology and nanostructure of homogeneous ethylene-1-octene (EO) copolymers can be tailored by varying the comonomer content [9,10]. Ethylene-1-octene copolymers exhibit lower densities and crystallinities than homogeneous ethylene copolymers of shorter α-olefins, in addition to lower glass transition temperatures, down to ultimately approx. −65 °C. Hence, from a basic point of view, the EO copolymers with high comonomer content represent an attractive model system for which the properties and the nanostructure of very low crystallinity polyethylene materials can be correlated.

The present paper offers a study of the microhardness behavior at room temperature of a series of EO copolymers with high comonomer content. The following issues will be emphasized: (i) the microhardness value of an EO copolymer having a very low density ($\rho = 0.848$ g/cm$^3$) is reported for the first time, and (ii) the nature of the deformation mechanism in low crystallinity materials with $T_g \ll$ RT is discussed, in contrast to that of semicrystalline systems with high degree of crystallinity, or non-crystalline polymers with $T_g >$ RT.

## 2. Experimental

### 2.1. Materials

Homogeneous EOM ethylene-1-octene copolymers with different comonomer contents were synthesized in a continuously stirred tank reactor (CSTR) using different, Boron-activated metallocenes [11]. Table 1 collects the short-chain branching content per 100 carbon atoms, as determined by Fourier transform infrared spectroscopy (FTIR) or nuclear magnetic resonance (NMR). The molar mass of the EOM samples in Table 1 is approximately the same, $M_w = 8.8 \times 10^4$ g/mol, the polydispersity being around 2. The granular material was introduced inside a metal ring of approx. 0.7 mm diameter and approx. 1 mm height on top of a glass slide placed on a Koffler stage. A second glass slide covered the ring and the sample from the upper side. The material was heated above its melting temperature and subsequently compressed by hand with help of a prism of approx. 2 cm height, which was used for isolating purposes. Finally, the sample was allowed to cool down to room temperature. The average cooling rate during crystallization was estimated to be within the range 10–40 °C/min. The highest cooling rate applies for samples with high crystallization temperatures, $T_c$ (approx. 80 °C), while the slowest crystallization rate corresponds to samples with $T_c$ around room temperature.

Homogeneous EOC ethylene-1-octene copolymers with different comonomer contents were supplied by Dow Chemical. The molar mass of the EOC samples lies within the range $M_w = 6 \times 10^4$–$12 \times 10^4$ g/mol. The polydispersity is around 2. The sample branching content was provided by the supplier (Table 1). The as received material was compression moulded between two glass slides at 160 °C and subsequently cooled to room temperature at 10 °C/min.

### 2.2. Density

Density values at 23 °C, see Table 1, are measured according to ISO 1183-1:2004, immersion method. The volume degree of crystallinity, $\alpha$, was determined from the

Table 1
Branching content ($CH_3$/100C), density at room temperature (23 °C), volume crystallinity from density ($\alpha$), crystal thickness from Ref. [9] ($l_c$), microhardness ($H$) and crystal microhardness values ($H_c$), for the ethylene-1-octene samples investigated

| Sample | $CH_3$/100C[a] | $\rho$ at 23 °C (g/cm$^3$)[b] | $\alpha$ | $l_c$ (nm) [Ref 9] | $H$ (MPa) | $H_c$ (MPa) |
|---|---|---|---|---|---|---|
| EOC1 | 1.24[c] | 0.910 | 0.416 | 4.5 | 13.1 ± 0.1 | 31.5 |
| EO2855M | 1.92[FTIR] | 0.908 | 0.403 | 3.9 | 11.2 ± 0.3 | 27.8 |
| EOC2 | 2.20[c] | 0.902 | 0.362 | 3.5 | 10.1 ± 0.1 | 27.9 |
| EO2711M | 2.36[FTIR] | 0.900 | 0.349 | 3.3 | 9.05 ± 0.08 | 25.9 |
| EOC3 | 3.14[c] | 0.868 | 0.134 | 3.1 | 2.0 ± 0.2 | 14.9 |
| EO2835M | 3.59[FTIR] | 0.880 | 0.215 | 3.1 | 3.4 ± 0.1 | 15.6 |
| EO2741M | 4.21[FTIR] | 0.871 | 0.154 | 3.0 | 2.18 ± 0.01 | 14.2 |
| EO2963M | 5.08[FTIR] | 0.859 | 0.074 | 3.0 | 0.53 ± 0.02 | 7.2 |
| EO4082M | 6.00[NMR] | 0.848 | 0.00 | – | 0.12 ± 0.02 | – |

[a] Including endgroups.
[b] According to ISO 1183-1:2004, immersion method.
[c] Provided by the supplier.

density values following

$$\alpha = \frac{\rho - \rho_a}{\rho_c - \rho_a} \quad (2)$$

where $\rho_c$ is the crystal density, assumed to be $\rho_c = 0.997$ g/cm$^3$ [12], and $\rho_a = 0.848$ g/cm$^3$ is taken as the density of the amorphous phase. We have adopted the $\rho_a$ value from the density value of the EO4082M sample, which did not reveal either X-ray or DSC crystallinity at RT (Table 1).

### 2.3. Differential scanning calorimetry (DSC)

Calorimetric measurements were carried out using a Perkin–Elmer DSC-7. The scans were performed within the range 34–120 °C, using a rate of 10 °C/min. Sample masses were typically approx. 4–6 mg. Indium was used for calibration purposes.

### 2.4. Atomic force microscopy (AFM)

An atomic force microscope (AFM, Digital Instruments, Dimension 3000 atomic force microscope equipped with Nanoscope IIIa controller) operating in Tapping Mode at room temperature was employed. The resonant frequency and spring constant of the super-sharp silicon cantilever were approximately 300 kHz and 15 N/m, respectively. The radius of curvature was about 10 nm. The ratio of set-point amplitude to the amplitude of free oscillation was approximately 0.7 (moderate tapping force). Height and phase images were simultaneously collected, although only the unfiltered phase images are presented in this paper.

Samples for AFM measurements were fine-trimmed using a Leica Ultramicrotome (Ultracut E) at a temperature of −120 °C by means of a diamond knife (Diatome company). The flat surface thus obtained, ≈70×70 μm, was scanned for the characterization of the sample morphology.

### 2.5. Microindentation hardness

Microhardness measurements were carried out at room temperature (23 °C) using a Vickers indenter attached to a Leitz tester. The Vickers indenter is a four sided pyramidal tip producing indents, square in shape. In order to minimize creep effects, the indenter penetrates the sample surface upon application of a given load for 6 s. For each applied load, the size of the residual impression was measured using an optical microscope. Microhardness values were determined from the linear regression of a $P$ vs. $d^2$ plot, where $P$ is the applied load and $d$ the indentation diagonal, following [2]:

$$H = 1.854P/d^2 \quad (3)$$

Three different loads in the range 49–245 mN are used for each sample, except for EO2963M and EO4082M. It is noteworthy that the extremely low hardness values of the latter samples (Table 1) give rise to very large indentation sizes for the smallest load available, even recognizable by eye (for EO4082M, $d \approx 0.9$ mm using $P = 49$ mN). Hence, the use of loads other than 49 mN was not feasible.

## 3. Results and discussion

### 3.1. Microhardness of low crystallinity ethylene-based materials

Fig. 1 illustrates the microhardness variation as a function of the degree of short-chain branching, for the series of ethylene-1-octene copolymers investigated (Table 1). For the sake of comparison, Fig. 1 also includes the range of hardness values typical for linear polyethylene samples ($H = 43$–90 MPa for zero branching), prepared under a variety of crystallization conditions and having molar masses in the range $5\times10^4$–$3\times10^5$ g/mol [13,14]. The solid line in Fig. 1 is a guide to the eye. The shaded area illustrates the range of microhardness values extrapolated for degrees of branching in the range 0–1.2%.

One can clearly observe that the microhardness value conspicuously decreases with increasing degree of branching. The largest $H$ value for the ethylene-1-octene series (13 MPa for 1.2% degree of branching) is substantially smaller than the typical values for linear polyethylene samples (43–90 MPa). Most interesting is the fact that the microhardness reduces to values as low as $H = 0.12$ MPa, for the sample with the highest branching content. Preceding microhardness studies on a series of branched PE samples, already evidenced the $H$ decreasing tendency with increasing branching content, however, the smallest $H$ value reported was approx. 4 MPa for a degree of branching of approx. 7% [15]. The smaller H values reported in the present paper are associated to the lower levels of crystallinity, as will be discussed below, due to the homogeneous distribution of the branches.

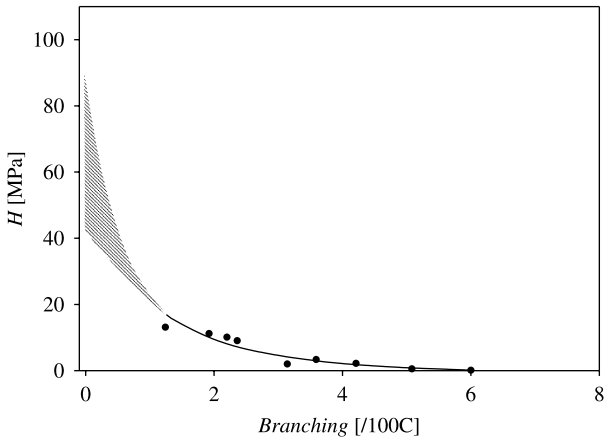


Fig. 1. Plot of microhardness as a function of the degree of short-chain branching (number of branches per 100 carbon atoms), for the ethylene-1-octene series. The solid line is a guide for the eye. The dashed area illustrates the range of $H$ values expected for 0–1.2% branching, from published data for linear PE samples [13,14].

### 3.2. Influence of short-chain branching on the degree of crystallinity

Fig. 2 shows the plot of the volume fraction crystallinity at room temperature as a function of the degree of short-chain branching, for the ethylene-1-octene series. The dashed area in Fig. 2 covers the range of $\alpha$ values anticipated for 0–1.2% of branching, considering the typical $\alpha$ values reported for linear polyethylene ($\alpha = 0.55$–$0.85$) [13,14]. Results reveal that the degree of crystallinity gradually decreases with increasing branching content, reaching $\alpha \approx 0$ for the highest branching content. Similar results have been previously observed in homogeneous ethylene-1-octene copolymers [10]. The latter study also suggests that there is a gradual change with increasing comonomer content from a lamellar based morphology into a granular one consisting of small, imperfect, blocky nanostructures, and possibly via fringed-micelles to clusters of loosely-packed ethylene sequences [10,16,17]. In addition, it was found that EO samples with $\rho$-values below roughly 0.870 g/cm$^3$ do not exhibit WAXS crystalline reflections either at room temperature or upon cooling at −60 °C. However, asymmetric WAXD patterns at −60 °C, due to very weak underlying crystalline reflections, are observed for samples having room temperature densities between 0.855 and 0.870 g/cm$^3$, indicating that these samples are not amorphous at −60 °C. Moreover, SAXS invariants were found to change upon heating and cooling, even for the sample with the highest degree of branching (44 mol% of 1-octene, approx. 15 branches per 100 (C) [10]. Hence, it seems that, even for EO copolymers with very high comonomer contents, nanostructures with slightly larger structural order than the amorphous surroundings are formed.

It is noteworthy that the EO series studied in the present paper exhibits DSC crystallinity at room temperature except for the sample with the highest branch content (EO4082M). In addition, our X-ray results confirm previous findings [10], which indicate that samples with $\rho < 0.870$ g/cm$^3$ do not exhibit WAXS reflections at room temperature. The small quantity and size of nanocrystals together with the imperfection of these crystalline nanostructures are presumably the reason why these structures cannot be detected by WAXS. However, a number of lamellar-like nanostructures can be observed in the AFM image of the sample having 7% crystallinity (Fig. 3). In addition, a large amount of granular clusters of ≈4 nm diameter appear to be homogenously distributed throughout the bulk of this sample. The same type of granular accumulations is also detected in the AFM image of the EOM sample with highest branching content (not shown). However, in this case there is no evidence of any lamellar-like nanostructure. These granular arrangements could be mainly related to regions of higher density within the amorphous phase, and to a lesser extent to a small amount of blocky imperfect 'nanocrystals'.

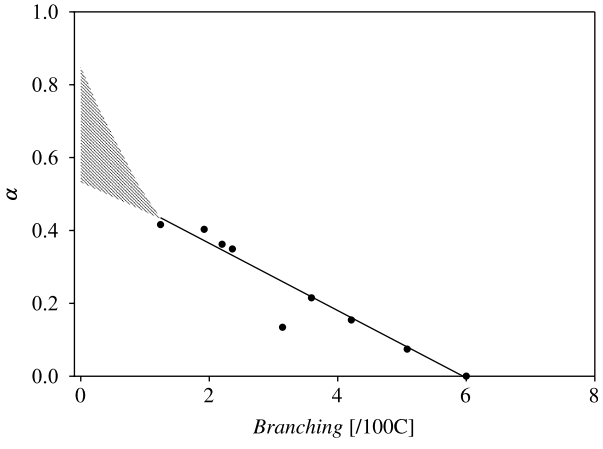


Fig. 2. Plot of degree of crystallinity vs. degree of short-chain branching for the ethylene-1-octene copolymers. The solid line and the dashed area have the same meaning as the ones drawn in Fig. 1.

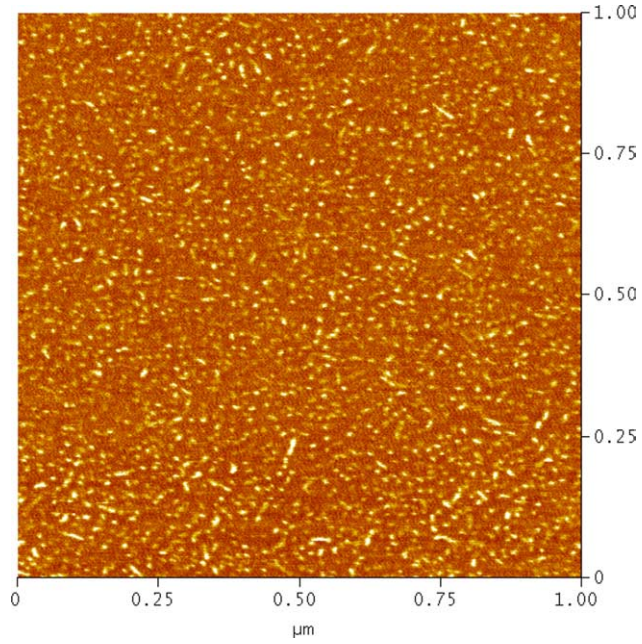


Fig. 3. AFM phase image of the inner surface of the EOM sample with 5.08% branching content (Table 1).

In the light of the foregoing X-ray, DSC and atomic force microscopy results, we have considered the degree of crystallinity for the EO4082M sample ($\rho = 0.848$ g/cm$^3$) to be of $\alpha \approx 0$ at RT. However, in principle, one cannot discard the occurrence of regions with slightly different electron density.

### 3.3. Microhardness-nanostructure correlation in low crystallinity PE systems

Fig. 4 shows the microhardness of the EO copolymer series as a function of the degree of crystallinity (solid symbols). Characteristic data for linear polyethylene (open symbols) have been included for comparison [13,14]. The data shown in Fig. 4 offers us the opportunity to discuss, for the first time, the $H$ behavior with $\alpha$ for PE-based systems with levels of crystallinity below 0.22. Let us first briefly recall the microhardness behavior with $\alpha$ for linear polyethylene. It is now well established and has been discussed in a number of papers that the microhardness of linear polyethylene samples ($\alpha > 0.4$) can

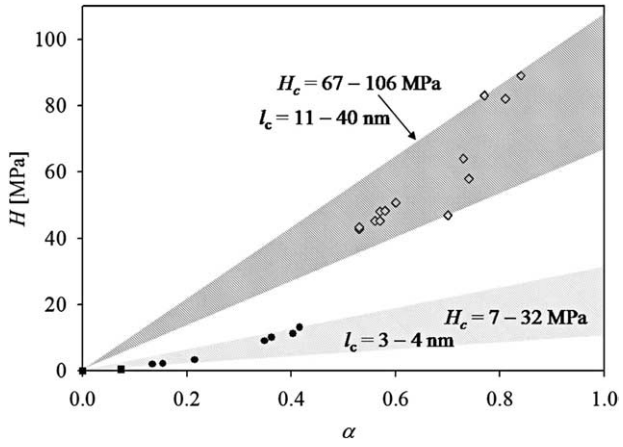


Fig. 4. Variation of microhardness with degree of crystallinity for the ethylene-1-octene copolymers (solid symbols). Typical data for linear PE's are included for comparison (open symbols). The shaded areas highlight the different $H-\alpha$ behaviour found for linear PE (dark area) and for highly short-chain branched PE samples (light area).

be explained in terms of the additive contribution of the crystalline and amorphous regions (Eq. (1)), where $H_a \approx 0$ [1,2,13,14]. The validity of the assumption of the microhardness value for amorphous material to be close to zero is now experimentally demonstrated, as $H = 0.12$ for EO4082M ($\alpha \approx 0$) (Fig. 4 and Table 1). Typical $H_c$ values for linear PE, as determined using Eq. (1), range from 67 to 106 MPa (see intersection of the dark shaded area with the right-hand $y$-axis in Fig. 4). These $H_c$ values satisfactorily correlate with the lamellar thickness, $l_c$, following [1,2]

$$H_c = \frac{H_c^{\infty}}{1 + (b/l_c)} \tag{4a}$$

where $H_c^{\infty} = 170$ MPa is the hardness of an infinitely thick PE crystal and the 'mechanical' parameter, $b = 2\sigma_e/\Delta h$, is related to the ratio between the surface free energy of the crystals, $\sigma_e$, and the energy required for plastic deformation, $\Delta h$.

Hence, the variability of the $H$ data for linear PE (Fig. 4) is a combination of: (i) the degree of crystallinity (Eq. (1)) and (ii) the $H_c$ value, which is eventually related to the $l_c$ and $b$ values (Eq. (4a)). The data shown under the dark shaded area exhibit $H_c$, $l_c$ and $b$ values, which are characteristic for linear PE ($H_c$ = 67–106 MPa, $l_c$ = 11–40 nm and $b$ = 18–26 nm) [13,14].

Fig. 4 additionally shows that $H$ for the EO samples follows a different trend with $\alpha$ as that shown for linear PE. Hence, a new light shaded area embraces the data for the short-chain branched samples. Comparison of the two shaded areas reveals that, for a given $\alpha$ value, the $H$ values are substantially smaller for the EO samples than for the linear PE ones. This result can be immediately explained as a consequence of the remarkably low $H_c$ values found for the ethylene-1-octene materials ($H_c$ = 7–32 MPa). Indeed, these $H_c$ values represent the smallest ones reported for a polymer crystal so far. What could be the reason for such unusual $H_c$ values? In the first place, the lamellar thicknesses for EO copolymers are significantly lower ($l_c$ = 3–4 nm [9]) than those of linear PE ($l_c$ = 11–40 nm). However, in case of the EO samples with the highest branch contents, the small $l_c$ values alone do not account for the large $H_c$ deviation observed and one should invoke variations in the $b$ parameter, partly associated to changes of the surface free energy of the crystals. As the comonomer content increases, and the density concomitantly decreases as mentioned before, not only the lamellar thickness decreases, but also the lateral dimensions will decrease drastically. For samples crystallized from the melt with $\rho \leq 870$ kg/m$^3$, a gradual change from a lamellar into a granular morphology takes place. In addition, the increasing comonomer content leads to various effects: firstly, the topology of the chains at the end surface will change from non-adjacent folding towards situations where steric impediments at the crystallite's surface arise. As a consequence, smaller crystallites with increased curvature; with large inclinations of the crystallite stems, and with bundle-type of associations as in case of fringed-micellar structures, should be expected. Thus, the end surface free energy of the crystals, $\sigma_e$, will tend to increase. Secondly, as the lateral dimensions ($a'$ and $b'$) decrease, the side surfaces of the lamellae, and consequently the side surface free energy of the crystals $\sigma_s$, will become comparable with that of the basal (end) surface. As a result, Eq. (4a) has to be modified into (assuming $b' \approx a'$)

$$H_c = \frac{H_c^{\infty}}{1 + (1/\Delta h)\left((2\sigma_e/l_c) + (4\sigma_s/a')\right)} = \frac{H_c^{\infty}}{1 + \left((b_e/l_c) + (2b_s/a')\right)} \tag{4b}$$

where $b_e = 2\sigma_e/\Delta h$; $b_s = 2\sigma_s/\Delta h$. In the case of a lamellar morphology, $b_e/l_c \gg 2b_s/a'$, and Eq. (4b) leads to Eq. (4a). For blocky nanocrystals, assuming $l_c \approx a' \approx b' \approx d$, Eq. (4b) can be rewritten as

$$H_c = \frac{H_c^{\infty}}{1 + (b/d)} \tag{4c}$$

where $b/d = (b_e + 2b_s)/d \approx (b_e/l_c) + 2b_s/a'$.

### 3.4. Microhardness behavior for materials with high short-chain branching content: the influence of the mechanical b-parameter

Fig. 5 illustrates the variation of the $b$-values as a function of branching content, for the ethylene-1-octene copolymers investigated in the present paper. The $b$-values were calculated with help of Eq. (4c), using the $H_c$ values as determined from Eq. (1) (Table 1), and the $d$ values ($\approx l_c$) previously published [9] for similar ethylene-1-octene copolymers (Table 1). The range of $b$-values typical for linear PE is also included for comparison. One sees that, initially, the $b$-values (for lamellar crystallites $b$ is given by $b_e = 2\sigma_e/\Delta h$) remain constant with increasing branch content. However, a conspicuous increase in the $b$-parameter is observed above 2% of branching, reaching a value of $b \approx 80$ nm (for blocky structures, $b = (2\sigma_e + 4\sigma_s)/\Delta h$) for the highest branching content. The remarkable $b$-increase for high comonomer content values is thus explained as due to a combination of: (a) an increase of the basal surface free energy of the crystals, $\sigma_e$; and (b) the contribution of the side surface free energy $\sigma_s$, due to the decreasing lateral dimensions

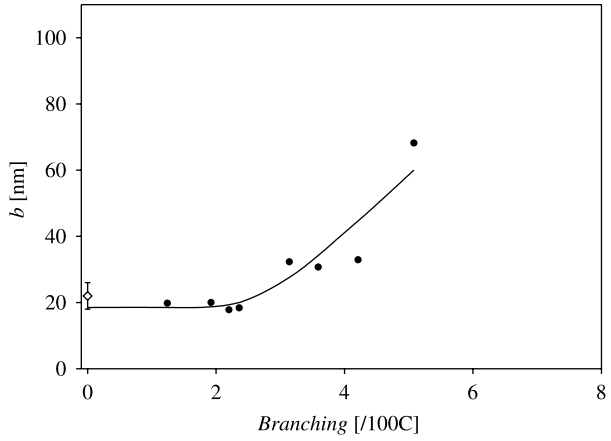


Fig. 5. Plot of the $b$-parameter as a function of short-chain branching content, for the EO materials (solid symbols). The typical $b$-value for linear PE has also been included (open symbol). The error bar associated to the $b$-value of linear PE relates to the dispersion of $b$-values found in the literature for a range of PE samples with different molar masses, prepared under various crystallization conditions [13,14].

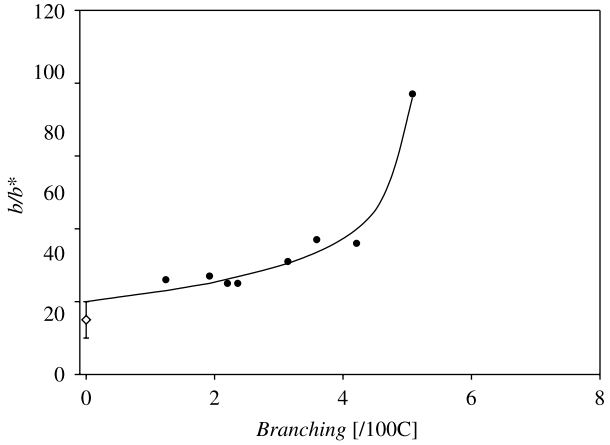


Fig. 6. Plot of the ratio between the mechanical $b$- and the thermodynamical $b^*$-parameters, as a function of short-chain branching content.

of the crystals (approaching the size of the longitudinal dimension). However, the $b$-increase at high branching contents could also be partly due to variations of the energy required for plastic deformation $\Delta h$. To shed more light on this issue, DSC measurements were carried out.

To derive the 'thermodynamical' $b^*$-value for each EO sample, we have used the well known Gibbs–Thomson equation

$$T_m = T_m^\infty \left(1 - \frac{b^*}{l_c}\right) \tag{5a}$$

where $T_m^\infty$ is the equilibrium melting point and $b^* = 2\sigma_e/\Delta h_f$, $\Delta h_f$ being the melting enthalpy. $b^*$ relates to the thermodynamical properties while $b$ depends on the mechanical behavior. If the thermodynamical $b^*$-parameter is taken as being analogous to the mechanical $b$-parameter, then the ratio $b/b^* = \Delta h_f/\Delta h$ is of interest [14]. Consequently, the study of the $b/b^*$ ratio as a function of branching content could provide a direct information about the $\Delta h$ behavior.

Analogous to the change of Eq. (4a) into (4b), Eq. (5a) has to be modified to account for the limited size of the lateral crystal dimensions in the case of blocky morphologies following (assuming $b' \approx a'$):

$$T_m = T_m^\infty \left(1 - \left(\frac{b_e^*}{l_c} + \frac{2b_s^*}{a'}\right)\right) \tag{5b}$$

For $l_c \approx a' \approx b' \approx d$, Eq. (5b) leads to

$$T_m = T_m^\infty \left(1 - \left(\frac{b^*}{d}\right)\right) \tag{5c}$$

where $b^*$ now relates to $(2\sigma_e + 4\sigma_s)/\Delta h_f$.

As in the case of lamellar morphology, $b/b^* = \Delta h_f/\Delta h$ is expected to reflect changes with respect to the $\Delta h$ behavior. In the following calculations, we have assumed $\Delta h_f = 250$ J/g for the EO copolymers and $\Delta h_f = 293$ J/g for the linear material [18]. Fig. 6 illustrates the plot of the ratio $b/b^*$ as a function of branching content for the samples investigated. The $b/b^*$ ratio significantly increases with increasing octene content above 2% branching, approaching a value of $b/b^* \approx 100$ and $\Delta h = 2.5$ J/g ($\Delta h_f = 250$ J/g) for the highest branching content. Thus, the $\Delta h$ value of 2.5 J/g is remarkably lower than that found for linear PE samples ($b/b^* \approx 35$, $\Delta h = 8.4$ J/g, using $\Delta h_f = 293$ J/g). This result suggests that the energy required for plastic deformation is substantially reduced in case of samples with very large degrees of branching.

### 3.5. Deformation mechanism model in very low crystallinity systems: the influence of a viscous amorphous phase

The foregoing results suggest that the response of highly branched PE to indentation is significantly different from that of linear PE. For moderate branching contents ($\leq 2.5\%$), the large deviation of $H$ from $H_c^\infty$ ($H/H_c^\infty = 0.05 - 0.08$; taking $H_c^\infty = 170$ MPa [13]) (Fig. 4), as compared to the usual $H$ values for linear PE ($H/H_c^\infty = 0.25 - 0.52$), is mainly due to: (i) the small degree of crystallinity ($\alpha \approx 0.35$–$0.40$) and (ii) the small crystal lamellar thickness ($l_c = 3.3$–$4.5$ nm). However, for high branching contents ($> 2.5\%$), the extremely small $H$ values ($H/H_c^\infty = 0.003 - 0.02$) obtained cannot be only explained as due to the small $\alpha$ and $l_c$ values ($\alpha = 0.07$–$0.22$, $l_c \approx 3$ nm). Thus, also large $b$-values must be invoked (Fig. 5). The large $b$-values are partly caused by the increasing surface free energies involved as the crystal lateral dimensions diminish, while there is a continuous change from lamellar crystallites, for which $b$ is given by $b_e = 2\sigma_e/\Delta h$, towards blocky structures with $b = (2\sigma_e + 4\sigma_s)/\Delta h$. In addition, however, the substantial $b$-increase could be associated with a decrease of the energy required for plastic deformation of the crystals (leading to $\Delta h_f/\Delta h \approx 100$), in contrast to the usual $\Delta h$ value for linear and low branched PE ($\Delta h_f/\Delta h \approx 35$). As a result, the deformation mechanism occurring in highly short-chain branched ethylene-based materials appears to differ substantially from that taking place in case of linear and low short-chain branched PE.

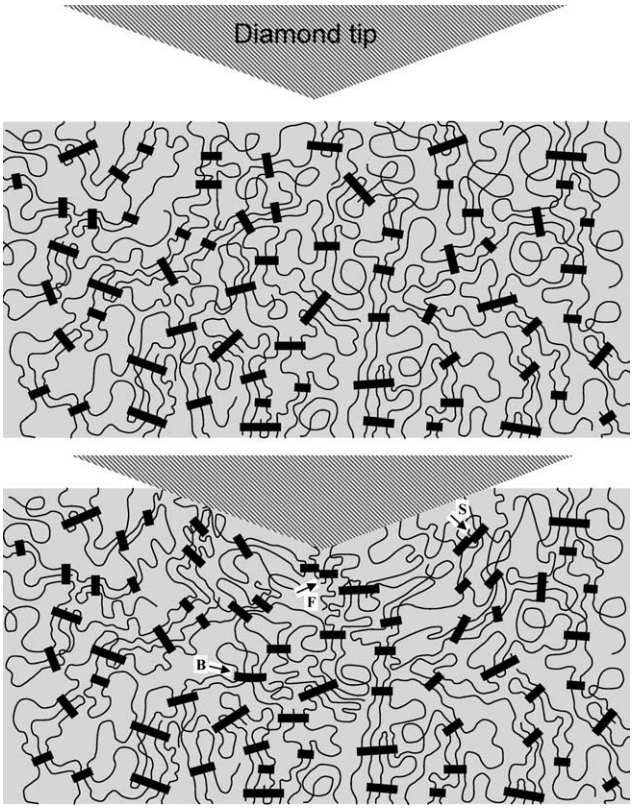


Fig. 7. Schematic illustration of the distribution of nanocrystals within the amorphous phase, for a highly branched ethylene-1-octene sample, at the following stages of an indentation cycle: (a), before indentation; (b), under applied load. Shearing (S), bending (B) and fracture (F) mechanisms of the nanocrystals are schematically depicted (see text).

EO copolymers with high degrees of branching (>2.5%) display very low levels of crystallinity ($\alpha = 0.07$–$0.22$). Consequently, here the small and imperfect nanocrystals are dispersed within a viscous amorphous phase ($T_g \approx -65$ °C). In these systems, the nanocrystals supposedly 'slide' easily within the amorphous matrix under the influence of the compressive stress of the indenter. This is expected to result in a remarkable viscoelastic character of the slippage deformation mechanism, as depicted schematically in Fig. 7. In contrast, in case of higher crystallinity systems (linear and low short-chain branched PE), shearing of lamellae and other mechanisms of plastic deformation of the lamellae occur (like lamellae fracture, etc.). According to this concept, the energy required to displace the nanocrystals within the amorphous phase in very low crystallinity materials should be substantially smaller than that necessary for plastic deformation of the efficiently packed crystalline lamellae alternated by thin amorphous layers, in support of the smaller $\Delta h$ values derived for highly branched materials with respect to linear and low branched PE.

In summary, four types of deformation mechanisms can be distinguished depending on the macroscopic density of the polyethylene sample, from low-density homogeneous copolymers to high density materials (note that the subdivision is a very schematic one while the morphologies change in a continuous way [16]):

(1) For density values $\rho \sim 0.85$ g/cm$^3$ ($\alpha \sim 0$) (fully amorphous PE), deformation occurs by compression of the non-crystalline material. The stress required for deformation of the amorphous molecular network above $T_g$ (very large indentations are clearly seen) involves displacement of large bundles of chain segments against local restraints of secondary forces and internal rotations.

(2) For low density values in the range $0.85 < \rho \leq 0.87$ g/cm$^3$, ($0 < \alpha \leq 0.22$) The morphology is expected to develop from clusters of loosely-packed ethylene sequences via fringed-micelles and granular structures into lamellae. Deformation is dominated by preferential compression of the disordered phase under the stress field of the indenter. However, the presence of nanocrystals randomly distributed within the amorphous phase constituting a network of physical crosslinks connected by bridging molecules induces a reinforcement of the material. Resistance to deformation occurs by bond rotation of the molecules within the amorphous phase on the one hand, elastic compression and bending (in case of lamellae) of the nanocrystals on the other [5]. In addition, a slippage mechanism similar to the one described above could also take place. The extent of the latter deformation mechanism should be modulated by the viscosity of the amorphous phase.

(3) For density values $0.87 < \rho \leq 0.91$ g/cm$^3$ ($\alpha \approx 0.35$–$0.4$), both the amorphous and the crystalline regions contribute significantly to the resistance to deformation. The deformation modes of the lamellar crystallites could be similar to those described below (point number 4). However, in this case, the small thickness of the crystallites is the feature that limits the material resistance to plastic deformation.

(4) For density values $\rho > 0.91$ g/cm$^3$ ($\alpha \geq 0.5$), the deformation modes of the crystals predominate. The hard elements are lamellae having substantial thicknesses (and large lateral dimensions). The mechanical properties are primarily determined by the large anisotropy of molecular forces within the crystal. The mosaic structure of blocks within the lamellar crystals introduces a specific weakness element, which permits chain slip to proceed faster at the block boundaries than inside the blocks. The weakest element of the semicrystalline polymer is the surface layer between adjacent lamellae, containing chain folds, free chain ends, tie molecules, etc.

Finally, it should be mentioned that a recent analysis of branched PE microhardness data suggests that the low experimental $H$ values observed can be explained by using negative values of $H_a$ (Eq. (1)) [19]. The negative $H_a$ values are derived from an extrapolation of a general $H - T_g$ relationship found for glassy materials ($T_g >$ RT) [19,20]. The idea behind this approach is to account for a so called 'floating effect' of the solid crystals in the soft component, analogous to the one described above. However, negative values of hardness do not have any sound physical meaning.

The model proposed in the present paper relies on a sound physical background for two main reasons: (i) the microhardness value for an ethylene-based material with $\alpha \approx 0$ ($H_a$) has been experimentally measured for the first time, yielding a value $H_a = 0.12$ MPa; (ii) the low $H$ values found for low crystallinity EO materials with $T_g <$ RT can be accounted for on the basis of a combination of small longitudinal and lateral dimensions; of high end and side surface free energies; and of small $\Delta h$ values arising from a deformation mechanism different from that of linear PE.

## 4. Conclusions

1. The microhardness of an ethylene-based material (a homogeneous ethylene-1-octene copolymer) having a crystallinity value $\alpha \approx 0$ has been measured for the first time yielding an $H$ value approaching zero ($H = 0.12$ MPa).
2. The microhardness values of the ethylene-1-octene copolymers are conspicuously smaller than those of linear PE.
3. For moderate short-chain branching contents ($1.2 < CH_3/100C < 2.5\%$; $0.90 < \rho \leq 0.91$ g/cm$^3$), the small $H$ values found ($H/H_c^\infty = 0.05 - 0.08$), as compared to the usual $H$ values for linear PE ($H/H_c^\infty = 0.25 - 0.52$), can be explained on the basis of: (i) small degrees of crystallinity ($\alpha \approx 0.35$–$0.40$) and (ii) very small crystal lamellar thicknesses ($l_c = 3.3$–$4.5$ nm).
4. For high short-chain branching contents ($CH_3/100C > 2.5\%$; $\rho \leq 0.87$ g/cm$^3$), the extremely small $H$ values ($H/H_c^\infty = 0.003 - 0.02$) are accounted for by very large values for the $b$-parameter ($b = 32$–$68$ nm), in addition to the very small $\alpha$ ($\alpha \leq 0.22$) and nanocrystal dimensions (of a few nanometers scale).
5. The substantial $b$-increase with increasing branching content above 2.5% (Fig. 5) is associated to: (i) increased surface free energies, including the basal surface energies and the lateral ones and (ii) a decrease of the energy required for plastic deformation of the nanocrystals, $\Delta h \approx 2.5$ J/g ($b/b^* \approx 100$, $\Delta h_f = 250$ J/g), with respect to $\Delta h \approx 8.4$ J/g in case of crystals from linear and low branched PE ($b/b^* \approx 35$ and $\Delta h_f = 293$ J/g).

In contrast with high crystallinity lamellar systems in which lamellar shearing and breaking predominates, a mechanism of deformation for highly branched materials is proposed in which the dispersed nanocrystals 'slide' within the amorphous matrix under the stress field of the indenter.

## Acknowledgements

The authors acknowledge the Ministerio de Educación y Ciencia (Grant No. FIS2004-01331), Spain, for the generous support of this investigation.

## References

[1] Baltá Calleja FJ. Trends Polym Sci 1994;2:419.
[2] Baltá Calleja FJ, Fakirov. Microhardness of polymers. Cambridge: Cambridge University Press; 2000.
[3] Benavente R, Pérez E, Quijada R. J Polym Sci, Part B: Polym Phys 2001; 39:277.
[4] Flores A, Baltá Calleja FJ, Attenburrow GE, Bassett DC. Polymer 2000; 41:5431.
[5] Baltá Calleja FJ. Adv Polym Sci 1985;66:117.
[6] Gourrier A, Gourrier MC, Riekel C. Macromolecules 2002;35:8072.
[7] García Gutiérrez MC, Gourrier A, Riekel C. J Macromol Sci Phys 2004; B43:267.
[8] Baltá Calleja FJ, Santa Cruz C, Asano T. J Polym Sci, Part B: Polym Phys 1993;31:557.
[9] Peeters M, Goderis B, Vonk C, Reynaers H, Mathot VBF. J Polym Sci, Part B: Polym Phys 1997;35:2689.
[10] Vanden Eynde S, Mathot VBF, Koch MHJ, Reynares H. Polymer 2000; 41:4889.
[11] Adriaensens PJ, Karssenberg FG, Gelan JM, Mathot VBF. Polymer 2003; 44:3483.
[12] Wunderlich B. Macromolecular Physics. Crystal structure, morphology, defects, vol. 1. New York: Academic Press; 1973.
[13] Bayer RK, Baltá Calleja FJ, Kilian HG. Colloid Polym Sci 1997; 275:432.
[14] Flores A, Baltá Calleja FJ, Bassett DC. J Polym Sci, Part B: Polym Phys 1999;37:3151.
[15] Baltá Calleja FJ, Martínez Salazar J, Čačković H, Loboda-Čačković J. J Mater Sci 1981;16:739.
[16] Mathot VBF, Scherrenberg RL, Pijpers MFJ, Engelen YMT. In: Hosoda S, editor. The new trends in polyolefin science and technology. Trivandrum (India): Publisher Research Signpost; 1996. p. 71.
[17] Hu W, Mathot VBF, Frenkel D. Macromolecules 2003;36:2165.
[18] Mathot VBF. In: Mathot VBF, editor. Calorimetry and thermal analysis of polymers, 5. New York: Hanser Publishers; 1994. p. 105 [chapter 5].
[19] Fakirov S, Krumova M, Rueda DR. Polymer 2000;41:3047.
[20] Boyanova M, Fakirov S. Polymer 2004;45:2093.